

Collisions of Majorana Zero Modes

Liang-Liang Wang,^{1,2} Wenjun Shao,^{1,2} and Jian Li^{1,2,*}

¹*School of Science, Westlake University, 18 Shilongshan Road, Hangzhou 310024, Zhejiang Province, China*

²*Institute of Natural Sciences, Westlake Institute for Advanced Study,
18 Shilongshan Road, Hangzhou 310024, Zhejiang Province, China*

(Dated: December 27, 2023)

We investigate the collisions of Majorana zero modes, which are presented as inter-soliton collisional events in fermionic superfluids with spin-orbit coupling. Our results demonstrate that, the zero energy splitting, induced by the overlapping of inter-soliton Majorana wave-functions upon collision, generates an effective repulsive force for Majorana states, which in turn protected themselves against into bulk excitation. As a result, the collision between solitons associated with Majorana zero modes appears to be repulsive and elastic, as they do not penetrate each other but instead repel without energy loss. As well, similar repulsive behavior is observed in collisions between soliton-induced and defect-pinned Majorana zero modes. Our research offers new insights into the features of Majorana fermions, and robustness in the collisions of Majorana zero modes bodes well for the prospects of topological quantum computation with a multitude of Majorana qubits.

Introduction.— Majorana zero modes (MZMs)[1–4] are exotic, neutral quasiparticles composed of the equivalent contributions of the particle and the hole. They are of fundamental scientific importance and could have profound technological applications for fault-tolerant quantum computation[5–8], quantum memory [9–13] and quantum random-number generation[14, 15]. Similar to the Bardeen-Cooper-Schrieffer (BCS) pairing mechanism between electron creation and annihilation[16], the mixing of the particle and hole results in the ground states doubly degenerate, and two MZMs then form a protected qubit that is not locally measurable[9]. These non-Abelian quasiparticles are believed to merge in topological superconducting and superfluid systems, including the interfaces of *s*-wave superconductor and topological insulator[17–22], intrinsic two-dimensional superconductors with *p*-wave pairing symmetry[23–26], as well as topological ferromagnetic metal chains[27–29]. After the realization of spin-orbit coupling (SOC) in ultracold gases[30–34], atomic fermionic superfluids enter the topological state, offering a disorder-free and highly controllable platform for studying Majorana physics[35–38].

MZMs appear within the cores of certain soliton excitations[39–41], where a phase kink across the dipole-like structure of the order parameter arises from the atomic phase imprinting techniques[42–44, 53]. These zero-energy states lead to the degeneracy of the many-body ground states, which hinges on the precise degeneracy of the MZMs in various soliton cores. Physically, soliton is a good candidate for the control and manipulation of Majorana qubits owing to its classical particle-like character[46], and networks of such topological excitations have been proposed for the progress of quantum computing[47–50]. Nevertheless, in the presence of multiple solitons, inter-soliton colliding events become possible[51] and overlapping between Majorana states within different solitons are expected to lift the Majorana state degeneracy to some degree, even may lead to

a complete breakdown. For the purposes of topological quantum computation, it is vital to figure out the stability of the MZMs in colliding processes.

In this Letter we address this question by observing soliton collisions in one-dimensional fermionic superfluids with SOC. The existence of MZMs within the solitons has important consequences for the physics of soliton collisions. Based on our numerical simulations with time-dependent Bogoliubov-de Gennes equation, we find that the soliton collision with MZMs appears repulsive and completely elastic, i.e., they do not penetrate each other but instead repel with a well distance that the soliton matters can be safely regarded as untouched. Thus the soliton matter interaction could be negligible and allow us to clearly identify the collisional nature of MZMs. We confirm that the overlapping of inter-soliton Majorana wave-functions upon collision lift the Majorana degeneracy from zero. Moreover, the energy splitting of the Majorana states creates an effective repulsive force for MZMs, which in turn protected themselves against into bulk excitation. We stress that this is distinct from other repulsion mechanisms considered previously. And, for a contrast, we also demonstrate that soliton collisions become increasingly inelastic as we tune the system into the topological trivial phase. We further reexamine the repulsive interaction in collisions between soliton-bound and defect-pinned Majorana states. Our results show that Majorana zero modes are not only topologically protected, but also self-protected. This provides new insights into the intrinsic nature of Majorana states and these unusual colliding properties may open an alternative way to detect and discriminate Majorana qubits for fault-tolerant topological quantum computations.

Theoretical model. – Our starting point is the description of dark soliton-collisions in one-dimensional spin-half fermionic superfluids with SOC. The one-dimensional setting ensures the dark solitons stable with respect to the snake instability[52, 53] and the SOC effect can be

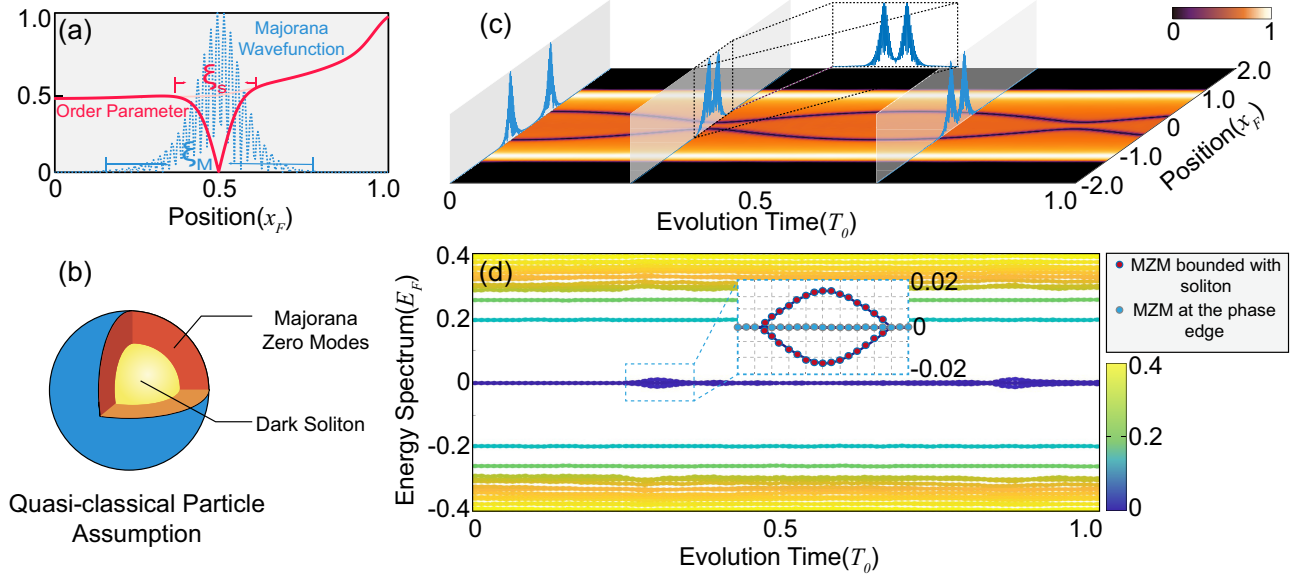


FIG. 1. (color online) (a) The solitonic pairing order parameter $\Delta(x)/E_F$ (solid red curve) and corresponding wave-function $|u_\uparrow(x)|$ (dashed blue curve) of the lowest-energy Majorana zero states inside the dark soliton at $x_0 = 0.5x_F$. (b) Quasi-classical illustration of the two-shell structure: dark soliton surrounded by Majorana wave-functions. (c) The evolution of the order parameter profile of the superfluid, while sequential snapshots of the lowest energy Majorana wave-functions (specifically $|u_\uparrow(x, t)|$) are displayed above it. The solitons begin at rest at a distance $\pm 0.5x_F$ from the trap centre. (d) Corresponding plot of the time dependent energy spectrum $E_\eta(t)$. Other parameters are $\alpha k_F = E_F$, $h_z = 1.0E_F$.

realized by two counter-propagating Raman lasers[31]. Within the standard mean-field framework, the dynamics of a fermionic superfluid can be modeled by the well-known time-dependent Bogoliubov-de Gennes (TDBdG) equation, whose one-dimensional form reads

$$\begin{bmatrix} H_0 & \Delta(x, t) \\ \Delta^*(x, t) & -\sigma_y H_0^* \sigma_y \end{bmatrix} \Phi_\eta(x, t) = i\hbar \frac{\partial}{\partial t} \Phi_\eta(x, t), \quad (1)$$

where the wave-functions is $\Phi_\eta \equiv [u_{\uparrow, \eta}, u_{\downarrow, \eta}, v_{\downarrow, \eta}, -v_{\uparrow, \eta}]^T$ in the Nambu representation. The single particle grand-canonical Hamiltonian has the form $H_0 = -\hbar^2 \partial_x^2 / 2m + m\omega^2 x^2 / 2 - i\alpha \hbar \partial_x \sigma_y - \mu + h_z \sigma_z$, describing the motion of fermionic atoms confined in a harmonic trapping potential with an oscillation frequency ω . α is the SOC strength, h_z the effective Zeeman field, and μ the chemical potential. The order parameter has the self-consistent form $\Delta(x, t) = g_{1D} \sum_\eta [u_{\uparrow, \eta}(x, t)v_{\downarrow, \eta}^*(x, t)f(-E_\eta) - u_{\downarrow, \eta}(x, t)v_{\uparrow, \eta}^*(x, t)f(E_\eta)]$ and the atom density function is given by $n_\sigma(x, t) = \sum_\eta |v_{\sigma, \eta}(x, t)|^2 f(-E_\eta) + |u_{\sigma, \eta}(x, t)|^2 f(E_\eta)$, where $g_{1D} = -2\hbar^2 / (ma_{1D})$ is the effective interatomic coupling given by an s -wave scattering length a_{1D} . $f(E) = 1/[e^{E/k_B T} + 1]$ is the Fermi-Dirac distribution at a temperature T , and the summation is over the quasi-particle state $E_\eta \geq 0$. Eq.(1) should be calculated self-consistently with the constraints of a fixed total atomic number $N = \int dx [n_\uparrow(x, t) + n_\downarrow(x, t)]$ and the above definition of the order parameter.

The particle-hole symmetry of BdG Hamiltonian ensures that MZMs only occur at exact zero energy and

typically localized in the vicinity of defects, such as phase edges or solitons. In this work, multiple dark solitons may be chosen to be *real* and π -phase kinks are introduced at the spots $\{x_i, i = 1, 2, 3, \dots\}$, given by

$$\Delta(x) = |\Delta(x)| \exp[i\pi \sum_i \Theta(x - x_i)], \quad (2)$$

where $\Theta(x)$ is the Heaviside step function. We seek the stationary solutions self-consistently with the use of Eq. (2), after a number of iterations up to convergence. When the local superfluid becomes topological[39], a pair of MZMs appear inside the soliton core and it is useful to note that the interaction between MZMs inside a dark soliton vanishes due to the intrinsic property of the dark soliton: a sharp phase jump. In dynamic simulations, we use a dimensionless interaction parameter to characterize the interaction strength, $\gamma = -mg_{1D}/\hbar^2 n$, which is basically the ratio between the interaction and kinetic energy at the density n . We choose the Fermi vector and energy, $k_F = \pi n/2$ and $E_F = \hbar^2 k_F^2 / 2m$, as the units of wave-vector and energy, respectively. In a trapped cloud with N atoms, it is convenient to use the peak density of a non-interacting Fermi gas in the Thomas-Fermi approximation at the trap center, $n = (2/\pi) \sqrt{Nm\omega}/\hbar$, although the Fermi cloud itself is an interacting gas. Throughout the work, we consider only zero temperature and take the interaction parameter $\gamma = \pi$, the total atomic number $N = 100$.

Collisions of Majorana zero modes.— We first prepare the system in the topological phase and then place two

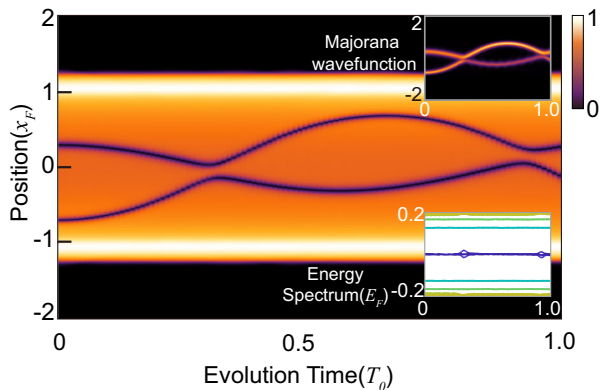


FIG. 2. (color online) Example of the evolution of an asymmetrical collision with two solitons prepared at $-0.8x_F$ and $0.3x_F$, respectively. The top inset shows the spatiotemporal contour plot of the Majorana wave-function, and bottom inset gives corresponding time dependent energy spectrum, where we can also observe the energy splitting in the collision.

dark solitons with a symmetrical displace, to observe the *head-on* collision at the trap centre. Majorana states emerge around the nodal point of the soliton, which is in contrast to bosonic superfluids, where the Gross-Pitaevskii solitons are structureless. The initial soliton separation $x_i = \pm 0.5x_F$ is large enough that the Majorana wave-function overlapping is negligible. Before the collision, a close inspection of the stationary dark soliton at $0.5x_F$ is shown in Fig.(1a). Owing to the appearance of MZMs within the soliton, the inter-soliton effects should be twofold: first, the mere soliton matter interaction arises sharply at spacings of the order of the soliton core width ξ_S , and second, the soliton-induced Majorana wave-function overlap with the length scale ξ_M , which describes the MZM behavior like $\sim \cos(\pi k_F x/2) \exp(-x^2/\xi_M^2)$. ξ_M is larger than ξ_S ($\xi_M \approx 2.5\xi_S$ in this case) and then we predict the Majorana soliton possesses a two-shell structure: soliton matter core surrounded by Majorana wave-functions (shown in Fig.(1b)). The collisions should be fascinating due to their multi-component nature.

In Fig.(1c), we present the evolution of the order parameter profile of the superfluid, while sequential snapshots of the lowest energy Majorana wave-functions (specifically $|u_\uparrow(x, t)|^2$) are displayed above it. Clearly, the resultant collision appears to be repulsive and elastic: the solitons slow down as they approach one another, come to a halt with a well distance of $\xi_{\min} \approx 0.3x_F$, and then reflect back to their original positions. With ($\xi_M > \xi_{\min} > \xi_S$), the soliton cores remain untouched and the Majorana wave-functions overlap (shown in Fig.(1c)). The soliton matter interaction could be negligible and thus we safely attribute the repulsive force just to the Majorana states, allowing us to clearly identify the nature of interactions between MZMs. To grasp the

main physics, the time dependent energy expectations $\langle E_\eta(t) \rangle = \langle \Phi_\eta(x, t) | H_{\text{BdG}}(x, t) | \Phi_\eta(x, t) \rangle$ are calculated to observe the energy splitting of zero modes in the collision, as shown in Fig. (1d). It's worth noting that, far away from each other, MZMs always have zero energy irrespective of the soliton velocity. As solitons get close enough, the zero modes split into a pair of levels ($E_0, -E_0$), which is proportional to the Majorana wave-function overlapping. This energy upshift creates a repulsive force for solitons that block their appropinquity and in turn drastically protects itself against scattering into bulk states. That's why the two solitons exhibit elastic collision only.

Moreover, asymmetrical collision is shown in Fig.(2). During collision, solitons exchange energy via the Majorana wave-function overlapping, hence, solitons with different velocities (increase the soliton speed by increasing x_i), the quantity of motion is preserved, i.e., the low-speed soliton after collision propagate with high velocity, while the high-speed one runs slowly, looks like passing through one another without changing form. The observed behavior of the above collision reveal that the Majorana states are not only topological protected, but also self-incurred protected, an aspect of the Majorana state that hadn't been explored before. This can ensure a more robust multi-Majorana quasiparticles transport.

Next, for a contrast, we tune the system into the topological trivial regime and observe the properties of the corresponding soliton collision. In Fig.(3), under the threshold $h_z \approx 0.7E_F$, the superfluid enter the topological trivial phase and finite energy Andreev-like bound states emerge near the point node of the soliton. Observably, inelastic soliton collision is presented and the lost energy is converted into small-amplitude density ripples that emanate from the point of the collision (shown in Fig.(3a)). Counter-intuitively, the dark solitons with lower energy have a higher velocity and vice versa, the soliton actually move faster after losing energy. Fig. (3b) shows the corresponding wave-function of lowest Andreev bound state (specifically $|u_\uparrow(x, t)|^2$). One can clearly see the corresponding ripples in the amplitude and, as a result, soliton-induced Andreev bound states are strongly up-shifted into the bulk quasi-particle scattering continuum, which eventually cause an emission of the sound and loss of the soliton energy (see Fig.(3c)). Furthermore, to quantify the elasticity of the collision, we evaluated the soliton speed discrepancy immediately before and after the first collisions with the decreasing Zeeman field in Fig.(3d). The phase diagram for occurrence of elastic and inelastic collisions is obtained, which strongly depends on the topological properties. The speed discrepancy rises suddenly around the transition point and the collisions become increasingly inelastic in topological trivial phase. The different collision properties between Majorana and Andreev solitons may lead to an interesting technique of soliton filter for distinguishing the Majorana states.

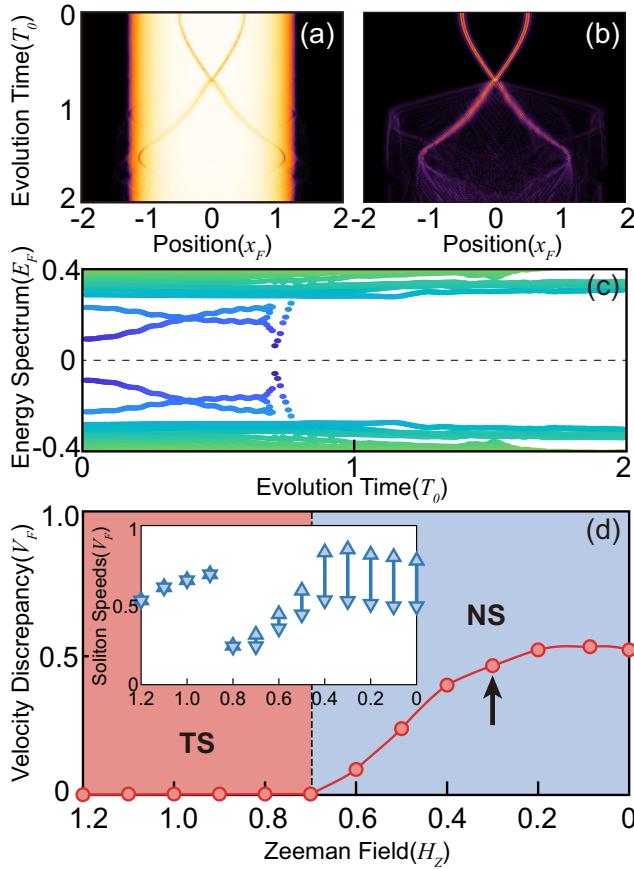


FIG. 3. (color online) (a-b) gives the collision of solitons in normal superfluid (NS) phase with $h_z = 0.3E_F$, where the left column (a) is the paring order parameter $\Delta(x, t)$, and the right one (b) shows the evolution of the lowest energy Andreev state (specifically $|u_\uparrow\rangle$). The collision is inelastic and the lost energy is converted into small amplitude ripples (shown both in (a) and (b)). As a result, soliton-induced Andreev states is up-shifted into the bulk quasi-particle scattering continuum, which is shown in (c). (d) The velocity discrepancy Δv between soliton velocity immediately before and after the first collisions as a function of Zeeman field h_z . In the normal superfluid (NS) phase, the velocity discrepancy increases from zero, denoting the collision is getting inelastic. As shown in the inset, blue downward (upward) pointing triangles are the soliton velocities before (after) the first collision.

Quasiclassical Analysis of Soliton Collision.— Dark soliton appear as wave packet that preserve its amplitude and shape during its propagation and even persist unchanged with MZMs in the colliding process, therefore being attributed as a particle-like character. In our study, the width of the Fermi cloud in the axial direction is much larger compared to the size of the soliton. Thus, under the local density approximation, the soliton can be treated as a macroscopic particle at coordinates q_i with p_i being generalized momentum. In our study, the overlapping between MZMs adjusts to the soliton’s motion and plays an important role in the soliton collision. According

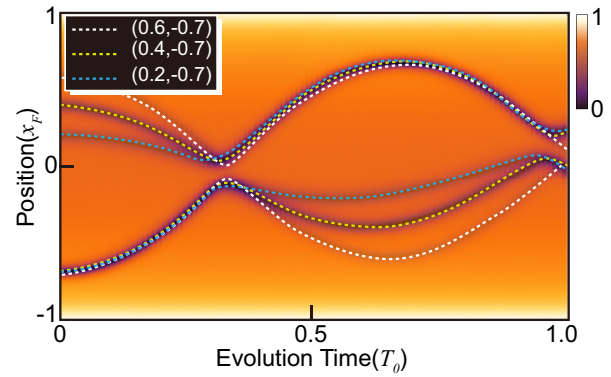


FIG. 4. (color online) Space-time plot of the asymmetric collisions with two solitons prepared at $(-0.7x_F, 0.2x_F)$, $(-0.7x_F, 0.4x_F)$ and $(-0.7x_F, 0.6x_F)$, respectively. The quasiclassical predictions of the soliton’s trajectories are highlighted with dashed lines, which show a good agreement with the numerical results.

to the energy splitting from zero $\propto \pm \exp(-|q_1 - q_2|/\xi_M)$ induced by the Majorana wave-function overlapping[55], their mutual repulsive potential can be assumed reasonably as $V(q_1, q_2) = Ae^{-|q_1 - q_2|/\sqrt{\xi_{M_1}\xi_{M_2}}}$, where A is the interaction intensity to be determined. The soliton matter interaction is negligible and we may finally obtain the Hamiltonian of the double solitons by evaluating the kinetic, trap and repulsive interaction energy terms in the absence of dissipation,

$$H(q_i, p_i) = \sum_{i=1,2} \frac{p_i^2}{2m_1^i} + \sum_{i=1,2} \frac{1}{2} m_S^i \omega^2 q_i^2 + V(q_1, q_2). \quad (3)$$

where m_1 is the inertial mass and $m_S = N_S m$ bare soliton mass, which can be determined in the snaking process of single soliton (as elaborated on in Supplementary Material). With the initial state $\{q_i(t=0) = x_i, p_i(t=0) = 0\}$, following the Hamiltonian equation of motion $\dot{q}_i = \partial H / \partial p_i$, $\dot{p}_i = -\partial H / \partial q_i$, the interaction intensity is fixed to be $A = 0.0137E_F$ compared with the soliton trajectory based on the full numerical BdG simulation in Fig.(2). The numerical results of the trajectories of the soliton centers and the time dependences of the soliton’s coordinates originating from Eq.3, are presented in Fig.(4) with different initial states. All the analytical results are in good agreement with the numerical data.

Collision with phase-edge Majorana states.— Then, in order to check the above-made statements and extend our works into the collision between MZMs within different topological defects, we perform numerical simulations of the collision between soliton-induced MZMs and one pinned at the phase edge. Due to the harmonic potential geometry, in a suitable parameter regime, a mixed phase emerges, consisting of a standard normal superfluid at the center and a topological superfluid at the

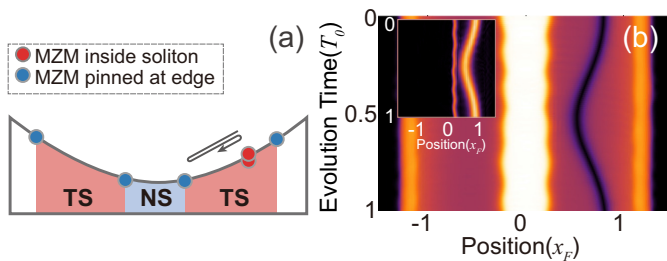


FIG. 5. (color online.) (a) A rough configuration of the system in a harmonic trap within the local-density approximation. From the center of the trap to the wings the phases are normal superfluid (NS) phase and topological superfluid (TS) respectively. (b) shows the dynamical evolutions of soliton in the TS region.

two edges of the trap[54], which is shown in Fig.(5a). A dark soliton was set in the topological region and accelerated by the trapping potential towards to the phase edge, where a MZM is prepared immovably. As shown in Fig.(5b), the soliton slow down as it approaches the phase edge at $0.2x_F$, and then turn back, performing a complete oscillation (a virtual phase edge reflection) inside the topological region. Or in other words, Majorana states hosted in the soliton has been limited in the span between two fixed MZMs, reminiscent of what has been observed in the soliton collision. The soliton behavior is generated by the conjunction of the trapping effect and repulsive interaction between Majorana states, which is an reconfirmation of the repulsive interaction of MZMs.

Conclusion.— To summarize, our study shows that the zero energy splitting, induced by the overlapping of inter-soliton Majorana wave-functions upon soliton collision, generates an effective repulsive force for Majorana states, which in turn protected themselves against into bulk excitation. A complete elastic collision takes place between solitons with Majorana states, which do not penetrate each other but instead repel without any loss of energy. Remarkably, our quasi-particle analysis can fully explain the numerical findings and provide a complete description of these anomalous behaviors with Majorana states. Additionally, we perform the investigation of the collisional mechanism between Majorana states within different topological defects to confirm our conjecture. Our research provides new insights into the features of Majorana fermions, and we envision that the robustness in the collisions of Majorana states could be utilized in the topological quantum computing with a network of Majorana qubits.

We thank An-chun Ji, Qing Sun and Changan Li for useful discussions. This work was supported by the foundation of Zhejiang Province Natural Science under Grant No. LQ20A040002 and JL acknowledges support from National Natural Science Foundation of China un-

der Project 11774317. The numerical calculations in this paper have been done on the super-computing system in the Information Technology Center of Westlake University.

* lijian@westlake.edu.cn

- [1] *Ettore Majorana*, edited by G. F. Bassani and the Council of the Italian Physical Society (Springer, Heidelberg, 2006).
- [2] F. Wilczek, “Majorana returns”, *Nat. Phys.* **5**, 614 (2009).
- [3] P. Brouwer, “Enter the Majorana Fermion”, *Science* **336**, 989 (2012).
- [4] S. Elliott, and M. Franz, “*Colloquium*: Majorana fermions in nuclear, particle, and solid-state physics”, *Rev. Mod. Phys.* **87**, 137 (2015).
- [5] M. Hasan and C. Kane, “*Colloquium*: Topological insulators”, *Rev. Mod. Phys.* **82**, 3045 (2010).
- [6] X. Qi and S. Zhang, “Topological insulators and superconductors”, *Rev. Mod. Phys.* **83**, 1057 (2011).
- [7] S. Tewari, S. Das Sarma, C. Nayak, C. Zhang, and P. Zoller, “Quantum Computation using Vortices and Majorana Zero Modes of a $p_x + ip_y$ Superfluid of Fermionic Cold Atoms”, *Phys. Rev. Lett.* **98**, 010506 (2007).
- [8] C. Nayak, S. Simon, A. Stern, M. Freedman, and S. Sarma, “Non-Abelian anyons and topological quantum computation”, *Rev. Mod. Phys.* **80**, 1083 (2008).
- [9] A. Kitaev, “Unpaired Majorana fermions in quantum wires”, *Physics-Uspekhi* **44**, 131 (2001).
- [10] A. Kitaev, “Fault-tolerant quantum computation by anyons”, *Annals of Physics* **303**, 2 (2003).
- [11] P. Shor, “Scheme for reducing decoherence in quantum computer memory”, *Phys. Rev. A* **52**, 2493(R) (1995).
- [12] M. Biercuk, H. Uys, A. VanDevender, N. Shiga, W. Itano, and J. Bollinger, “Optimized dynamical decoupling in a model quantum memory”, *Nature (London)* **458**, 996 (2009).
- [13] P. Maurer, G. Kucsko, C. Latta, L. Jiang, N. Yao, S. Bennett, F. Pastawski, D. Hunger, N. Chisholm, M. Markham, D. Twitchen, J. Cirac, and M. Lukin, “Room-temperature quantum bit memory exceeding one second”, *Science* **336**, 1283 (2012).
- [14] J. Rarity, P. Owens, and P. Tapster, “quantum random-number generation and key sharing”, *J. Mod. Opt.* **41**, 2435 (1994).
- [15] D. Deng, and L. Duan, “Fault-tolerant quantum random-number generator certified by Majorana fermions”, *Phys. Rev. A* **88**, 012323 (2013).
- [16] J. Bardeen, L. Cooper, J. Schrieffer, “Theory of Superconductivity”, *Phys. Rev.* **108**, 1175 (1957).
- [17] L. Fu, and C. Kane, “Superconducting proximity effect and Majorana fermions at the surface of a topological insulator”, *Phys. Rev. Lett.* **100**, 096407 (2008).
- [18] R. Lutchyn, J. Sau, and S. Sarma, “Majorana Fermions and a Topological Phase Transition in Semiconductor-Superconductor Heterostructures”, *Phys. Rev. Lett.* **105**, 077001 (2010).
- [19] Y. Oreg, G. Refael, and F. Oppen, “Helical Liquids and Majorana Bound States in Quantum Wires”, *Phys. Rev. Lett.* **105**, 177002 (2010).

- [20] J. Alicea, Y. Oreg, G. Refael, F. Oppen, and M. Fisher, “Non-Abelian statistics and topological quantum information processing in 1D wire networks”, *Nat. Phys.* **7**, 412 (2011).
- [21] L. Jiang, T. Kitagawa, J. Alicea, A. Akhmerov, D. Pekker, G. Refael, J. Cirac, E. Demler, M. Lukin, and P. Zoller, “Majorana Fermions in Equilibrium and in Driven Cold-Atom Quantum Wires”, *Phys. Rev. Lett.* **106**, 220402 (2011).
- [22] V. Mourik, K. Zuo, S. M. Frolov, S. R. Plissard, E. P. A. M. Bakkers, and L. P. Kouwenhoven, “Signatures of Majorana Fermions in Hybrid Superconductor-Semiconductor Nanowire Devices”, *Science* **336**, 1003 (2012).
- [23] N. Read, and D. Green, “Paired states of fermions in two dimensions with breaking of parity and time-reversal symmetries and the fractional quantum Hall effect”, *Phys. Rev. B* **61**, 10267 (2000).
- [24] T. Mizushima, M. Ichioka, and K. Machida, “Role of the Majorana Fermion and the Edge Mode in Chiral Superfluidity near a p -Wave Feshbach Resonance”, *Phys. Rev. Lett.* **101**, 150409 (2008).
- [25] K. Björnson, and A. M. Black-Schaffer, “Probing vortex Majorana fermions and topology in semiconductor/superconductor heterostructures”, *Phys. Rev. B* **91**, 214514 (2015).
- [26] J. M. Murray, and O. Vafek, “Majorana bands, Berry curvature, and thermal Hall conductivity in the vortex state of a chiral p -wave superconductor”, *Phys. Rev. B* **92**, 134520 (2015).
- [27] S. Nadj-Perge, I. K. Drozdov, B. A. Bernevig, and A. Yazdani, “Proposal for realizing Majorana fermions in chains of magnetic atoms on a superconductor”, *Phys. Rev. B* **88**, 020407 (2013).
- [28] J. Li, H. Chen, I. K. Drozdov, A. Yazdani, B. A. Bernevig, and A. H. MacDonald, “Topological superconductivity induced by ferromagnetic metal chains”, *Phys. Rev. B* **90**, 235433 (2014).
- [29] R. Pawlak, M. Kisiel, J. Klinovaja, T. Meier, S. Kawai, T. Glatzel, D. Loss, and E. Meyer, “Probing Atomic Structure and Majorana Wavefunctions in Mono-Atomic Chains on Superconducting Pb-Surface”, *npj Quantum Information*, **2**, 16035 (2016).
- [30] Y. Lin, K. Jiménez-García, and I. Spielman, “Spin-orbit-coupled Bose-Einstein condensates”, *Nature(London)* **471**, 83 (2011).
- [31] P. Wang, Z. Yu, Z. Fu, J. Miao, L. Huang, S. Chai, H. Zhai, and J. Zhang, “Spin-Orbit Coupled Degenerate Fermi Gases”, *Phys. Rev. Lett.* **109**, 095301 (2012).
- [32] Z. Wu, L. Zhang, W. Sun, X. Xu, B. Wang, S. Ji, Y. Deng, S. Chen, X. Liu, and J. Pan, “Realization of two-dimensional spin-orbit coupling for Bose-Einstein condensates”, *Science* **354**, 83 (2016).
- [33] Z. Meng, L. Huang, P. Peng, D. Li, L. Chen, Y. Xu, C. Zhang, P. Wang, and J. Zhang, “Experimental Observation of a Topological Band Gap Opening in Ultracold Fermi Gases with Two-Dimensional Spin-Orbit Coupling”, *Phys. Rev. Lett.* **117**, 235304(2016).
- [34] L. Huang, Z. Meng, P. Wang, P. Peng, S.-L. Zhang, L. Chen, D. Li, Q. Zhou, and J. Zhang, “Experimental realization of two-dimensional synthetic spin-orbit coupling in ultracold Fermi gases”, *Nat. Phys.* **12**, 540 (2016).
- [35] J. Dalibard, F. Gerbier, G. Juzeliūnas, and P. Öhberg, “Colloquium: Artificial gauge potentials for neutral atoms”, *Rev. Mod. Phys.* **83**, 1523 (2011).
- [36] F. Wu, G. Guo, W. Zhang, and W. Yi, “Unconventional Superfluid in a Two-Dimensional Fermi gas with Anisotropic Spin-Orbit Coupling and Zeeman fields”, *Phys. Rev. Lett.* **110**, 110401 (2013).
- [37] J. Devreese, J. Tempere, and C. Melo, “Effects of Spin-Orbit Coupling on the Berezinskii-Kosterlitz-Thouless Transition and the Vortex-Antivortex Structure in Two-Dimensional Fermi Gases”, *Phys. Rev. Lett.* **113**, 165304 (2014).
- [38] H. Zhai, “Degenerate quantum gases with spin-orbit coupling: a review”, *Rep. Prog. Phys.* **78**, 026001 (2015).
- [39] Y. Xu, L. Mao, B. Wu, and C. Zhang, “Dark Solitons with Majorana Fermions in Spin-Orbit-Coupled Fermi Gases”, *Phys. Rev. Lett.* **113**, 130404 (2014).
- [40] X.-J. Liu, “Soliton-induced Majorana fermions in a one-dimensional atomic topological superfluid”, *Phys. Rev. A* **91**, 023610 (2015).
- [41] A. M. Mateo and X. Yu, “Two types of dark solitons in a spin-orbit-coupled Fermi gas”, *Phys. Rev. A* **105**, L021301 (2022).
- [42] J. Denschlag, J. E. Simsarian, D. L. Feder, C. W. Clark, L. A. Collins, J. Cubizolles, L. Deng, E. W. Hagley, K. Helmerson, W. P. Reinhardt, S. L. Rolston, B. I. Schneider, and W. D. Phillips, “Generating Solitons by Phase Engineering of a Bose-Einstein Condensate”, *Science* **287**, 97 (2000).
- [43] S. Burger, K. Bongs, S. Dettmer, W. Ertmer, K. Sengstock, A. Sanpera, G. V. Shlyapnikov, and M. Lewenstein, “Dark Solitons in Bose-Einstein Condensates”, *Phys. Rev. Lett.* **83**, 5198 (1999).
- [44] B. P. Anderson, P. C. Haljan, C. A. Regal, D. L. Feder, L. A. Collins, C. W. Clark, and E. A. Cornell, “Watching Dark Solitons Decay into Vortex Rings in a Bose-Einstein Condensate”, *Phys. Rev. Lett.* **86**, 2926 (2000).
- [45] M. J. H. Ku, B. Mukherjee, T. Yefsah, and M. W. Zwierlein, “Cascade of Solitonic Excitations in a Superfluid Fermi gas: From Planar Solitons to Vortex Rings and Lines”, *Phys. Rev. Lett.* **116**, 045304 (2016).
- [46] Y. V. Kartashov, B. A. Malomed, and L. Torner, “Solitons in nonlinear lattices”, *Rev. Mod. Phys.* **83**, 247 (2011).
- [47] G. El, and A. Kamchatnov, “Kinetic Equation for a Dense Soliton Gas”, *Phys. Rev. Lett.* **95**, 204101 (2005).
- [48] H. Teras, D. Solnyshkov, and G. Malpuech, “Topological Wigner Crystal of Half-Solitons in a Spinor Bose-Einstein Condensate”, *Phys. Rev. Lett.* **110**, 035303 (2013).
- [49] M. Shaukat, E. Castro, and H. Teras, “Quantum dark solitons as qubits in Bose-Einstein condensates”, *Phys. Rev. A* **95**, 053618 (2017).
- [50] M. Ezawa, “Non-Abelian braiding of Majorana-like edge states and topological quantum computations in electric circuits”, *Phys. Rev. B* **102**, 075424 (2020).
- [51] R. Scott, F. Dalfovo, L. Pitaevskii, S. Stringari, O. Fialko, R. Liao and J. Brand, “The decay and collisions of dark solitons in superfluid Fermi gases”, *New J. Phys.* **14**, 023044 (2012).
- [52] J. Brand, and W. Reinhardt, “Solitonic vortices and the fundamental modes of the “snake instability”: Possibility of observation in the gaseous Bose-Einstein condensate”, *Phys. Rev. A* **65**, 043612 (2002).
- [53] M. Ku, B. Mukherjee, T. Yefsah, and M. Zwierlein, “Cascade of Solitonic Excitations in a Superfluid Fermi gas:

- From Planar Solitons to Vortex Rings and Lines”, *Phys. Rev. Lett.* **116**, 045304 (2016).
- [54] X. Liu, and P. Drummond, “Manipulating Majorana fermions in one-dimensional spin-orbit-coupled atomic Fermi gases”, *Phys. Rev. A* **86**, 035602(2012).
- [55] M. Cheng, R. Lutchyn, V. Galitski, and S. Sarma, “Splitting of Majorana-Fermion Modes due to Intervortex Tunneling in a $p_x + ip_y$ Superconductor”, *Phys. Rev. Lett.* **103**, 107001(2009).

Supplemental Material for “Collisions of Majorana Zero Modes”

Liang-Liang Wang,^{1,2} Wenjun Shao,^{1,2} and Jian Li^{1,2,*}

¹*School of Science, Westlake University, 18 Shilongshan Road, Hangzhou 310024, Zhejiang Province, China*

²*Institute of Natural Sciences, Westlake Institute for Advanced Study, 18 Shilongshan Road, Hangzhou 310024, Zhejiang Province, China*

(Dated: December 27, 2023)

In this Supplementary Material, we present the self-consistent time-splitting technique for the TDBdG equation, and show the asymmetric collision between solitons.

A. The self-consistent time-splitting technique for the TDBdG equation

In Fig. (S1), we sketch the self-consistent time-splitting technique for the TDBdG equation. We prepared the initial states by solving the self-consistent stationary BdG equation numerically. The following iterative algorithm is taken: one starts with an initial guess with the phase kink for the gap parameter, and then calculates the $u_{\sigma,\eta}$'s and $v_{\sigma,\eta}$'s by the diagonalization of the Hermitian BdG matrix. The corresponding $\Delta(x)$ is calculated by using the self-consistent order parameter equation, and iterated until pre-set convergence. We have to truncate the summation over energy levels η . This is done by introducing a high energy cut-off E_c . Once the stationary state is calculated, one moves to the solution of the time dependent BdG equation to simulate the soliton dynamics. We consider the standard splitting technique with self-consistency that approximates the evolution during a small time step dt . By firstly evolving the $[u_{\uparrow,\eta}(x, t_i), u_{\downarrow,\eta}(x, t_i), v_{\uparrow,\eta}(x, t_i), v_{\downarrow,\eta}(x, t_i)] \Rightarrow [u'_{\uparrow,\eta}(x, t_i), u'_{\downarrow,\eta}(x, t_i), v'_{\uparrow,\eta}(x, t_i), v'_{\downarrow,\eta}(x, t_i)]$ with the kinetic energy and spin-orbit coupling during dt ,

$$i\hbar \frac{\partial}{\partial t} \begin{bmatrix} u_{\uparrow,\eta} \\ u_{\downarrow,\eta} \\ v_{\uparrow,\eta} \\ v_{\downarrow,\eta} \end{bmatrix} = \begin{bmatrix} \hat{k}_x^2/2 & -i\lambda\hat{k}_x & 0 & 0 \\ i\lambda\hat{k}_x & \hat{k}_x^2/2 & 0 & 0 \\ 0 & 0 & -\hat{k}_x^2/2 & i\lambda\hat{k}_x \\ 0 & 0 & -i\lambda\hat{k}_x & -\hat{k}_x^2/2 \end{bmatrix} \begin{bmatrix} u_{\uparrow,\eta} \\ u_{\downarrow,\eta} \\ v_{\uparrow,\eta} \\ v_{\downarrow,\eta} \end{bmatrix}, \quad (\text{S1})$$

the above equation can be calculated in the momentum space by the Fourier transform, where

$$\begin{bmatrix} u'_{\uparrow,\eta} \\ u'_{\downarrow,\eta} \end{bmatrix} = \frac{1}{2} \begin{bmatrix} -i & i \\ 1 & 1 \end{bmatrix} \text{ifft} \left\{ \begin{bmatrix} A_1 & 0 \\ 0 & A_2 \end{bmatrix} \begin{bmatrix} i & 1 \\ -i & 1 \end{bmatrix} \text{fft} \left\{ \begin{bmatrix} u_{\uparrow,\eta} \\ u_{\downarrow,\eta} \end{bmatrix} \right\} \right\} \\ \begin{bmatrix} v'_{\uparrow,\eta} \\ v'_{\downarrow,\eta} \end{bmatrix} = \frac{1}{2} \begin{bmatrix} i & -i \\ 1 & 1 \end{bmatrix} \text{ifft} \left\{ \begin{bmatrix} B_1 & 0 \\ 0 & B_2 \end{bmatrix} \begin{bmatrix} -i & 1 \\ i & 1 \end{bmatrix} \text{fft} \left\{ \begin{bmatrix} v_{\uparrow,\eta} \\ v_{\downarrow,\eta} \end{bmatrix} \right\} \right\}, \quad (\text{S2})$$

with the matrix elements are $A_1 = e^{-idt(\hat{k}^2/2+\lambda\hat{k})}$, $A_2 = e^{-idt(\hat{k}^2/2-\lambda\hat{k})}$, $B_1 = e^{-idt(-\hat{k}^2/2+\lambda\hat{k})}$, $B_2 = e^{-idt(-\hat{k}^2/2-\lambda\hat{k})}$. After the renewed wavefunctions are obtained, we then update the order parameter through

$$\Delta'(x, t_i) = -g_{1D} \sum_{\eta} [u'_{\uparrow,\eta}(x, t_i)v'_{\downarrow,\eta}(x, t_i)f(-E_{\eta}) + u'_{\downarrow,\eta}(x, t_i)v'_{\uparrow,\eta}(x, t_i)f(E_{\eta})] \quad (\text{S3})$$

for the next procedure. The $[u'_{\uparrow,\eta}(x, t_i), u'_{\downarrow,\eta}(x, t_i), v'_{\uparrow,\eta}(x, t_i), v'_{\downarrow,\eta}(x, t_i)] \Rightarrow [u_{\uparrow,\eta}(x, t_i+dt), u_{\downarrow,\eta}(x, t_i+dt), v_{\uparrow,\eta}(x, t_i+dt), v_{\downarrow,\eta}(x, t_i+dt)]$ are evolved with the spatial part of the matrix during dt , where

$$i\hbar \frac{\partial}{\partial t} \begin{bmatrix} u'_{\uparrow,\eta} \\ u'_{\downarrow,\eta} \\ v'_{\uparrow,\eta} \\ v'_{\downarrow,\eta} \end{bmatrix} = \begin{bmatrix} C_{\uparrow} & 0 & 0 & \Delta(x, t) \\ 0 & C_{\downarrow} & -\Delta(x, t) & 0 \\ 0 & -\Delta^*(x, t) & -C_{\uparrow} & 0 \\ \Delta^*(x, t) & 0 & 0 & -C_{\downarrow} \end{bmatrix} \begin{bmatrix} u'_{\uparrow,\eta} \\ u'_{\downarrow,\eta} \\ v'_{\uparrow,\eta} \\ v'_{\downarrow,\eta} \end{bmatrix}, \quad (\text{S4})$$

with $C_{\uparrow} = V(x) - \mu - h_z$, $C_{\downarrow} = V(x) - \mu + h_z$ and $\Delta(x, t_i) = \Delta'(x, t_i)$. As we all know, $\Delta(x, t)$ is not a fixed but time dependent order parameter. According to the self-consistent condition, it exactly preserves the unitary of the wavefunctions during the entire evolution, but taking a fixed value of $\Delta(x, t_i)$ during the second step of the evolution

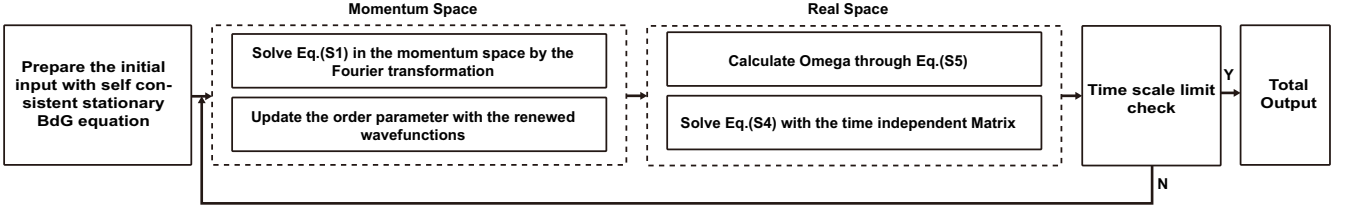


FIG. S1: (color online) Schematic flow chart for the self-consistent time-splitting technique of the TDBdG equation.

obviously breaks the indispensable self-consistency between Δ and $u_{\sigma,\eta}, v_{\sigma,\eta}$. Therefore the total number of particles is conserved to first order in the time step but not to all orders in dt . We go beyond the standard splitting method by resorting the self-consistency in the evolution during dt . With a simple analysis

$$\begin{aligned}
 i\hbar \frac{\partial}{\partial t} \Delta(x, t) &= -i\hbar \frac{\partial}{\partial t} \sum_{\eta} g_{1D} [u_{\uparrow,\eta}(x, t)v_{\downarrow,\eta}^*(x, t)f(-E_{\eta}) + u_{\downarrow,\eta}(x, t)v_{\uparrow,\eta}^*(x, t)f(E_{\eta})] \\
 &= \left[2(V(x) - \mu) - g_{1D} \sum_{\eta} (|v_{\downarrow,\eta}|^2 - |u_{\uparrow,\eta}|^2) f(-E_{\eta}) + (|v_{\uparrow,\eta}|^2 - |u_{\downarrow,\eta}|^2) f(E_{\eta}) \right] \Delta(x, t),
 \end{aligned} \tag{S5}$$

we fortunately find that $\Omega \equiv 2(V(x) - \mu) - g_{1D} \sum_{\eta} (|v_{\eta}|^2 - |u_{\eta}|^2) f(-E_{\eta}) + (|v_{\uparrow,\eta}|^2 - |u_{\downarrow,\eta}|^2) f(E_{\eta})$ is time independent with zero temperature. Thus the Eq. S4 can be transformed with $u_{\sigma,\eta}(x, t) = U_{\sigma,\eta}(x, t)e^{-i\Omega(x)t/2}$ and $v_{\sigma,\eta}(x, t) = V_{\sigma,\eta}(x, t)e^{i\Omega(x)t/2}$ and then evolve the $[U_{\sigma,\eta}(x, t), V_{\sigma,\eta}(x, t)]$ with the time independent 4×4 matrix. We sketch the self-consistent time-splitting procedure in Fig. (S1). It is clear that, about 1000 $\{u_{\uparrow}, u_{\downarrow}, v_{\uparrow}, v_{\downarrow}\}$ ' have to be simultaneously solved in the process, the computing task is rather demanding.

B. Quasi-classical properties of the soliton in the system

Here we consider the single soliton in a trapped Fermi superfluid, which preform a stable oscillation as a classical particle. Thus, under the local density approximation (LDA), the soliton can be treated as a macroscopic particle at position X with $V = dX/dt$ being the soliton velocity. For the dark soliton with phase-jump, it can be seen as a surface (or domain wall) in the Fermi gas. The associated surface tension (or the soliton energy) $E_s(\mu, V^2) \equiv E_{\text{withsoliton}}(\mu, V^2) - E_{\text{withoutsoliton}}(\mu)$ can be a function of the chemical potential μ and V^2 . Under the LDA, in the

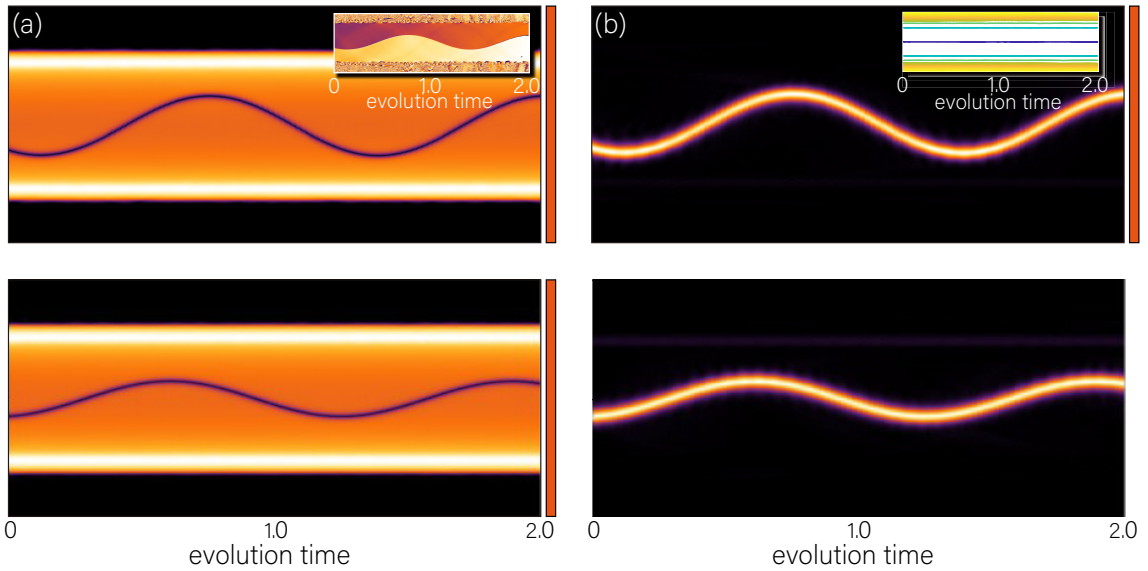


FIG. S2: (color online) Schematic flow chart for the self-consistent time-splitting technique of the TDBdG equation.

harmonic trap, we can say that $\mu(X) = \mu - U(X)$. According to the numerical results, the dark soliton with Majorana zero modes preserve their amplitude and shape during propagation and even persist elastic from collisions with one another. The energy conversion in the absence of dissipation gives

$$\frac{\partial E_s}{\partial t} = \frac{\partial E_s}{\partial \mu(X)} \cdot \frac{d\mu(X)}{dX} \cdot \frac{dX}{dt} + \frac{\partial E_s}{\partial V^2} \cdot \frac{dV^2}{dV} \cdot \frac{dV}{dt} = 0. \quad (\text{S6})$$

We define the inertial mass and the soliton particle number

$$m_I = 2 \frac{\partial E_s}{\partial V^2}, N_s = -\frac{\partial E_s}{\partial \mu(X)} = \int \left(-\frac{\partial H_s}{\partial \mu(X)} \right) - \left(-\frac{\partial H_0}{\partial \mu(X)} \right) dX = \int [n_s(x) - n_0(x)] dx, \quad (\text{S7})$$

in which $n_s(x)$ is the density with dark soliton and $n_0(x)$ is the density without the dark soliton. The quantity N_s is the deficit of the particles associated with the depression in the density at the soliton position. Note that, for dark solitons typically, $m_I < 0$ and $N_s < 0$. Hence, the Equation of the energy conservation gives

$$m_I \frac{dV}{dt} = -N_s \frac{dU}{dX} = -N_s m \omega_x^2 X. \quad (\text{S8})$$

For small amplitude oscillations, the soliton inertial mass is $m_I = N_s m [T_s/T_x]^2$, where $T_x = 2\pi/\omega_x$ and T_s is the soliton period, which can be obtained by the numerical data. Via the result shown in Fig. (S2), we can determine the value of T_s and N_s , then we can give the soliton inertial mass by the above relationship.

* Electronic address: lijian@westlake.edu.cn

[1] H.-R. Chen, K.-Y. Lin, P.-K. Chen, N.-C. Chiu, J.-B. Wang, C.-A. Chen, P.-P. Huang, S.-K. Yip, Y. Kawaguchi, and Y.-J. Lin, Phys. Rev. Lett. **121**, 113204 (2018).